Chemical routes to materials

CrossMark

Preparation of the all-solid-state Z-scheme WO$_3$/Ag/AgCl film on glass accelerating the photodegradation of pollutants under visible light

Hongbiao Fang[1] , Xin Cao[2] , Jiajie Yu[3] , Xiang Lv[1] , Nan Yang[1] , Tianhe Wang[2,*] , and Wei Jiang[1,*]

[1] *National Special Superfine Powder Engineering Center, Nanjing University of Science and Technology, Nanjing 210094, China*
[2] *State Key Laboratory of Advanced Technology for Float Glass, Bengbu 233000, China*
[3] *Chemicobiology and Functional Materials Institute, Nanjing University of Science and Technology, Nanjing 210094, China*

ABSTRACT

Tungsten oxide (WO$_3$) is a well-known photocatalyst, but its application is restricted due to its low conduction band and reduction power. In addition, WO$_3$ catalyst in powder forms has little application prospect because of difficulties in separation and regeneration. In this work, we prepared WO$_3$/Ag/AgCl films on conventional glass that not only have much enhanced photocatalytic capability but also can be readily regenerated. The WO$_3$ film was prepared on glass substrate by calcination of spin-coated W precursor. Ag/AgCl particles were then deposited on WO$_3$ film by an impregnating–precipitation–photoreduction method. The photocatalytic efficiency of WO$_3$/Ag/AgCl was evaluated by using methyl orange (MO) and Rhodamine B (RhB) as target pollutants. The highest photocatalytic performance was achieved with the 3-WO$_3$/Ag/AgCl film, being 18 and 13 times higher than that of pure WO$_3$ film for degradation of MO and RhB, respectively. The degradation rate for both MO and RhB by 3-WO$_3$/Ag/AgCl film catalyst decreased by less than 5% after five cycled tests. The photodegradation mechanism was discussed based on the electrochemical impedance spectroscopy Nyquist tests, photoelectrochemical analysis and reactive oxygen species scavenging experiments. A possible all-solid-state Z-scheme mechanism is proposed based on the photoelectron chemical tests and radical trapping experiments. This study provides a feasible technique to prepare a photocatalytic film with practicability and reproducibility.

Address correspondence to E-mail: thwang56@126.com; superfine_jw@126.com

Introduction

Modern industrial developments are increasingly facing challenges of environmental pollution and energy shortage. Water pollution is one of the most concerned problems [1–3]. Water contaminations are mostly caused by organic dyes released from various manufacturing processes including the textile and paper industries. Photocatalysis is an environment-friendly and effective method capable of degrading most organic pollutants. Considerable efforts have been made to develop economic and efficient photocatalysts that can fully utilize the solar light [4]. Multitudinous nanostructured semiconductors such as TiO_2 [5], Bi_2O_3 [6], SnO_2 [7] and ZnO [8] have been widely studied for photocatalytic degradation of organic pollutants in water under the sunlight irradiation. TiO_2 is one of the most studied photocatalyst because of its high stability, low cost and universal availability [9–11]. However, the large band gap (3.2 eV) of TiO_2 limits its utilization of solar energy to only about 5% (UV region), and this, in turn, restrains its practical applications [12–14]. Recently, photocatalysts with narrow band gaps that can sufficiently utilize visible light energy have been intensively explored.

Tungsten trioxide (WO_3) is a promising material because of its lower band gap (2.4–2.8 eV), high oxidation potential of valence band (VB) holes (+ 3.1–3.2 eV vs SHE), and it absorbs blue part of the solar spectrum [12, 15–17]. WO_3 has been used in many fields like photocatalysts, gas sensors, photochromic devices and electrocatalysts because of its chemical and thermal stability [18–21]. However, the photocatalytic efficiency of pure WO_3 is extremely low due to its low conduction band. Therefore, it has poor ability to react with electron acceptors such as oxygen and has high rate of the photo-generated electron–hole pairs [22, 23]. For these reasons, many methods have been developed to extend the photo-response region of semiconductor or promote the separation of the photo-generated electrons and holes [24, 25]. There have been several reported techniques to improve the photocatalytic performance of WO_3 such as noble metal loading, surface sensitization and metal or nonmetal element doping [26–28]. Among them, doping with noble metal (i.e., gold, platinum and silver) is an effective way to enhance the absorption of sunlight and improve the photocatalytic efficiency. Recently, novel plasmonic Ag/AgX

(X = Cl, Br, I) photocatalysts have been investigated because of its excellent photocatalytic performance under visible light, and Ag/AgCl was one of the most studied among them [29, 30]. The absorption range of Ag/AgCl in the region of visible light is broadened because of the surface plasmon resonance (SPR) effect of Ag [31, 32]. However, pure Ag/AgCl has the relatively low reducibility and is also relatively expensive, thus restricting its practical application. As an excellent photocatalyst, Ag/AgCl has been reported to modify other semiconductor photocatalysts, such as TiO_2 [14], C_3N_4 [33], BiOX [34] and $BiVO_4$ [35]. Ag nanoparticles (Ag NPs) have been used to improve the properties of the WO_3. Gao et al. [36] prepared the Ag/WO_3 films based on wood, and it could enhance negative oxygen ions production properties under visible light. Hashemi et al. [37] fabricated the WO_3/Ag/WO_3 multilayer nano-films through a physical vapor deposition method and studied the effects of annealing temperature on the optical properties and microstructural variation of films.

However, most of WO_3/Ag/AgCl photocatalysts reported in the previous literature are in powder form, thus having little aspects for practical applications because tedious regeneration is required. Ma et al. [38] prepared the Ag–AgCl/WO_3 hollow sphere with flower-like structure which had superior visible photocatalytic activity because of its unique morphology. Adhikari et al. [39] developed the Ag/AgCl/WO_3 powder by microwave-assisted hydrothermal method, and the photocatalytic activity of WO_3 was greatly enhanced. WO_3/Ag/AgCl film catalysts can overcome this problem and significantly reduce the regeneration cost. To our best knowledge, preparation of WO_3/Ag/AgCl film on a conventional glass substrate has not been reported elsewhere.

In this work, WO_3 film was spin-coated on glass substrate using tungstic acid as precursor, hydrogen peroxide as solvent and polyvinyl alcohol 124 as adhesive. Ag/AgCl was incorporated onto WO_3 film by impregnating–precipitation–photoreduction method [40, 41]. The photocatalytic performance of the WO_3/Ag/AgCl film was experimentally evaluated by the photodegradation of MO and RhB under visible light. The results show that the WO_3/Ag/AgCl film photocatalysts had excellent photocatalytic capability. In addition, this photocatalyst was stable and could be repeatedly used without showing any obvious deterioration. An all-solid-state Z-scheme photocatalytic

mechanism for the $WO_3/Ag/AgCl$ film was proposed based on the photoelectrochemical experiments, valence band analysis and trapping experiments.

Materials and methods

Materials

Tungstic acid (H_2WO_4, 99.95%), polyvinyl alcohol 124 [(C_2H_4O)n, GR], hydrogen peroxide 30% (H_2O_2, AR), sodium chloride (NaCl, AR), silver nitrate ($AgNO_3$, AR), methyl orange (MO, 96%) and Rhodamine B (RhB, AR) were purchased from Aladdin, Shanghai. Silicate glass was used as the substrate, and deionized water was used in all experiments.

Preparation of WO_3 film

The WO_3 film on glass substrate was prepared by heating tungstic acid at high temperature, and a typical procedure is as follows: 1.0 g tungstic acid was added in 20 mL hydrogen peroxide 30% under stirring at room temperature. Meanwhile, 0.5 g polyvinyl alcohol 124 was dropped with stirring for 24 h. The obtained tungstic acid solution was spin-coated on a silicate glass slide at 500 rev/min for 5 s. Prior to use, the silicate glass pieces were cut in 15 mm × 20 mm in size and cleaned successively with detergent, and deionized water. The as-coated substrates were dried in an oven at 85 °C for 1 h, and then calcinated in a furnace at 600 °C for 4 h to allow WO_3 to be sintered on the glass.

Fabrication of $WO_3/Ag/AgCl$ film

Impregnating–precipitation–photoreduction method was used to incorporate Ag/AgCl onto WO_3 film. The as-prepared WO_3 was immersed in 20 mL 0.005 mol/L $AgNO_3$ solution for 10 min. Next, the sample was dipped in 20 mL 0.0005 mol/L NaCl solution for 10 min and then flushed with the deionized water. The above immersion procedure was repeated for three times to precipitate AgCl onto WO_3. Afterward, the sample was dried in an oven. In a similar way, $WO_3/Ag/AgCl$ film samples were prepared with 0.01 mol/L and 0.02 mol/L of $AgNO_3$ and NaCl solutions. Finally, the above samples were irradiated under 100 W Hg lamp for 10 min. The as-

prepared samples were donated as 1-WO_3/Ag/AgCl, 2-WO_3/Ag/AgCl and 3-WO_3/Ag/AgCl representing samples prepared with concentration of $AgNO_3$ and NaCl solutions 0.005 mol/L, 0.01 mol/L and 0.02 mol/L, respectively.

Materials characterization

The crystal phase structures were measured by X-ray diffraction (XRD) equipped with Cu Kα radiation (λ = 0.1541 nm) operated at 40 kV and 40 mA. UV–Vis spectra of these samples was obtained with UV–Vis spectrophotometer (Shimadzu UV 2600) with $BaSO_4$ as the reflectance stand. The surface and cross-sectional morphology of the film was analyzed by scanning electron microscopy (SEM, HITACHI S-4800, Japan) equipped with an energy dispersive X-ray spectroscopy (EDS) to characterize the chemical composition. The microstructure of the optimized sample was observed HRTEM using a JEOL 2010 microscope operated at 200 kV. The X-ray photoelectron spectroscopy (XPS) on an RBD-upgraded PHI-5000C ESCA system (Perkin-Elmer) with Mg Kα radiation (hv = 1253.6 eV) was used to investigate on the chemical composition and electronic binding energy of the photocatalysts. All binding energies were calibrated against the C 1s binding energy at 284.6 eV of the surface adventitious carbon. Electrochemical performance was measured by an electrochemical workstation (CH660E, China) based on a conventional three-electrode system.

Photocatalytic activity

The photocatalytic performance of these samples was evaluated by degradation of MO and RhB (5 mg/L) under visible light. A 300-W Xe arc lamp with a 420-nm cutoff filter was used in all experiments, and the intensity of our photocatalytic test was 40 mW/cm^2. Each experimental process was conducted as follows: Two pieces of the prepared samples were placed in a 50 mL glass container equipped with 30 mL of MO and RhB (5 mg/L) aqueous solution. The glass container was equipped with cooling water circulator and placed where the distance between the light source and aqueous solution was 15 cm. The two pieces of the prepared samples were submerged in the aqueous solution for 30 min in the dark to achieve adsorption/desorption equilibrium. 2 mL of aqueous solution was taken out at every 30 min and

was measured by UV–Vis spectroscopy (UV 2600) to determine the pollutant concentration. The aqueous solution was carefully returned into the reactor after measured. In order to ascertain the main active substances in $WO_3/Ag/AgCl$ system, the degradation test was carried out with different scavengers. Among the scavengers, isopropyl alcohol (IPA) was used as ·OH scavenger, 1, 4-benzoquinone (BQ) was h^+ scavenger and ethylenediaminetetraacetic acid disodium salt (EDTA-2Na) was $·O_2^-$ scavenger [42–45].

Photoelectrochemical experiment

The photoelectrochemical performances of samples were investigated on a CHI660E electrochemical workstation using a standard three-electrode system. During the experiment, 0.5 M Na_2SO_4 solution was used as electrolyte. A platinum wire, a saturated calomel electrode (SCE) and the FTO glass (15×20 mm) coated with WO_3 and $WO_3/Ag/AgCl$ film were used as counter, reference and working electrodes, respectively. The EIS was tested at the open-circuit potential with the frequency range from 0.1 to 10^5 Hz. The magnitude of the modulation signal was set to 5 mV. The transient photocurrent responses of the samples were determined under inconsecutive illumination by 300-W Xe arc lamp with a UV-cutoff filter ($\lambda \geq 420$ nm) via five on–off cycles. During the experiment, the electrolyte was 0.5 M Na_2SO_4 solution.

Results and discussion

Optical photograph of the films

Figure 1 shows the digital photographs of the as-prepared film photocatalysts on the glass substrates. Both WO_3 and $WO_3/Ag/AgCls$ appear uniform and transparent. Slight decrease in transparency was observed with the increase in $AgNO_3$ and NaCl concentrations. 3-$WO_3/Ag/AgCl$ showed the pale brown appearance but maintained its transparency.

Structure, composition and morphology

The crystalline phases of the as-prepared samples were identified by XRD. The XRD pattern was acquired from the powder carefully scratched off from the coating on the glass substrates by using the ceramic blade. Figure 2 presents the XRD pattern of these film photocatalysts. From Fig. 2, the diffraction of WO_3 matched well with the JCPDS card NO. 43-1035 and WO_3 exhibited the major peaks, which was indexed to the typical monoclinic structure of WO_3. As for the $WO_3/Ag/AgCl$, in addition to the peaks of WO_3, additional XRD pattern peaks appeared at 27.8°, 32.3°, 46.3°, 54.8°, 57.5° and 76.7°, corresponding to the (111), (200), (220), (311), (222) and (420) planes of AgCl (JCPDS card NO. 31-1238) [46–48], respectively. Besides, no additional crystalline peaks were observed, manifesting the high purity of the obtained samples. The peaks of Ag were not observed in $WO_3/Ag/AgCl$, and the possible reason was that the amount of Ag was so small that it was beyond the detection limit of the XRD. As for $WO_3/Ag/AgCl$ film, with the increase in $AgNO_3$ and NaCl contents, the main peaks of AgCl gradually enhanced, indicating that the amount AgCl
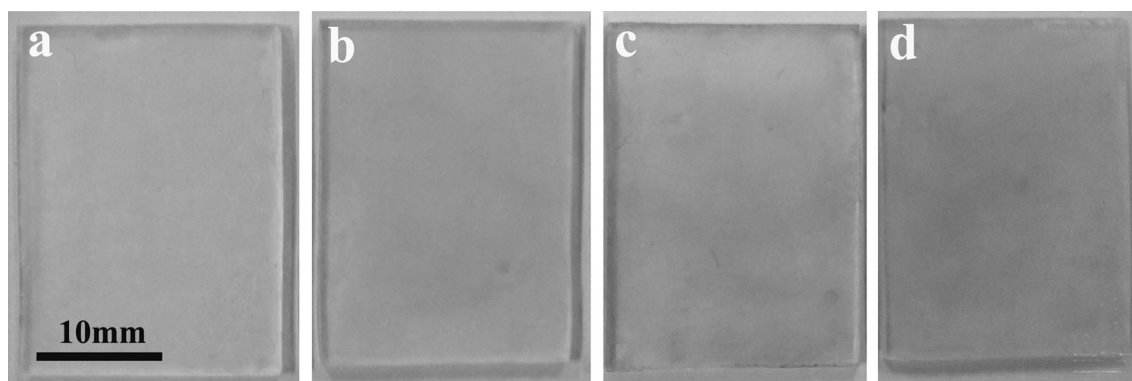

Figure 1 Digital photographs of pure WO_3 (**a**), 1-$WO_3/Ag/AgCl$ (**b**), 2-$WO_3/Ag/AgCl$ (**c**) and 3-$WO_3/Ag/AgCl$ films (**d**).
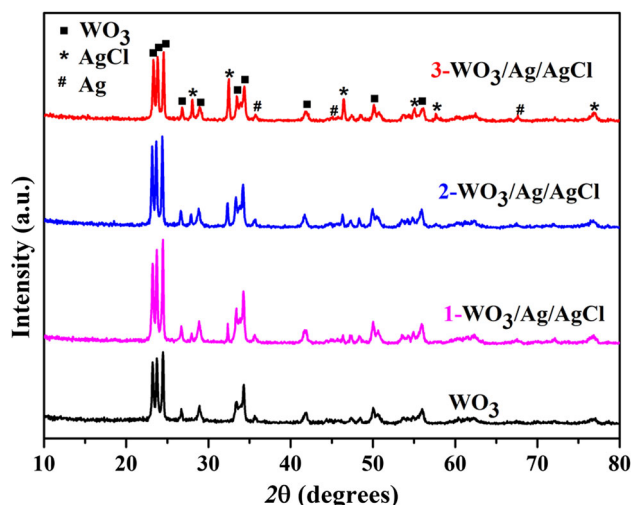
Figure 2 XRD patterns of the as-prepared samples.

increased. By using the Debye–Scherrer equation, it was possible to estimate the crystallite sizes for WO_3, Ag and AgCl. Table 1 summaries the crystallite sizes for WO_3, Ag and AgCl calculated from the strongest signal.

The morphology of the as-prepared samples calcined at 600 °C was examined by SEM. As shown in Fig. 3a, b, the WO_3 crystals were adhered firmly on the surface of silicate glass. This film could not be peeled off by sonicating it in the ethanol or water. The crystals were uniformly distributed on the surface of glasses and were not stacked to each other. As shown in Fig. 3c–h, the Ag and AgCl particles were well attached to the surface of WO_3 and glass. The sizes of Ag (90 nm) and AgCl (300 nm) particles were larger than that calculated from the XRD, probably due to the agglomeration of these crystals. Apparently, the distribution densities of Ag and AgCl particles increased with the $AgNO_3$ and NaCl concentration. For the WO_3/Ag/AgCl film, as shown in Fig. 3h, the AgCl particles with a diameter of about 300 nm were uniformly distributed on the surface of WO_3 film.

Table 1 The crystallite sizes of WO_3, Ag and AgCl calculated by the Debye–Scherrer equation from the strongest signal

	WO_3/nm	Ag/nm	AgCl/nm
1-WO_3/Ag/AgCl	46.74	71.79	51.74
2-WO_3/Ag/AgCl	43.71	42.32	55.29
3-WO_3/Ag/AgCl	43.21	42.32	81.30
Pure WO_3	36.86		

The elemental composition of WO_3 and 3-WO_3/Ag/AgCl was further investigated by the EDS profile, and the result is shown in Fig. 4a, b. For WO_3, O and W were detected from WO_3, Ca from glass and Au from the test. The element composition of W, Ag, Cl and O were detected on WO_3/Ag/AgCl film. These results confirmed that these samples were not contaminated by other chemical species. The distribution of chemical elements on the surface of 3-WO_3/Ag/AgCl was further characterized by EDX element mapping, as shown in Fig. 4c. It is apparent that the Ag and AgCl particles were evenly distributed on the surface of WO_3 film, which would benefit for steering charge flow and enhancing the separation and migration of the photo-generated charge between WO_3 and Ag/AgCl.

Figure 5 shows the TEM, HRTEM and cross-sectional SEM images of 3-WO_3/Ag/AgCl film. It is noted that WO_3, Ag and AgCl were in contact with each other as shown in Fig. 5a. As shown in Fig. 5b, the lattice fringe spacing with value of 0.384 nm was corresponding to the (002) lattice plane of monoclinic WO_3. Meanwhile, it is clearly recognized that the lattices of 0.236 nm and 0.277 nm were consisting with the (111) plane of Ag and the (200) plane of AgCl, respectively. [36]. According to the above results, the WO_3 and Ag/AgCl were closely attached with each other and highly crystalline, which was in consistent with the result of XRD. It is noted that the film thickness was around 1.35 μm, as shown in Fig. 5c.

Figure 6 shows the optical properties of WO_3 and three WO_3/Ag/AgCl films detected by UV–Vis diffuse reflectance spectra. The WO_3 film shows the absorption edge at about 450 nm, which was in accordance with the band gap of about 2.7 eV as reported previously [49, 50]. In comparison, WO_3/Ag/AgCl photocatalysts demonstrated wider and broader absorption spectra in 500–800 nm region of visible light, suggesting that the red shift of absorption spectra was due to the surface plasmon resonance (SPR) effect of Ag nanoparticles that were photoreduced from AgCl. Furthermore, the absorption intensity of samples both in UV and visible regions increased with the amount of Ag/AgCl particles on the surface of WO_3. The WO_3/Ag/AgCl composites with the enhanced absorption ability indicate that the responsive light range can be broadened and have the potential to have better photocatalytic efficiency. The inset in Fig. 6 shows the
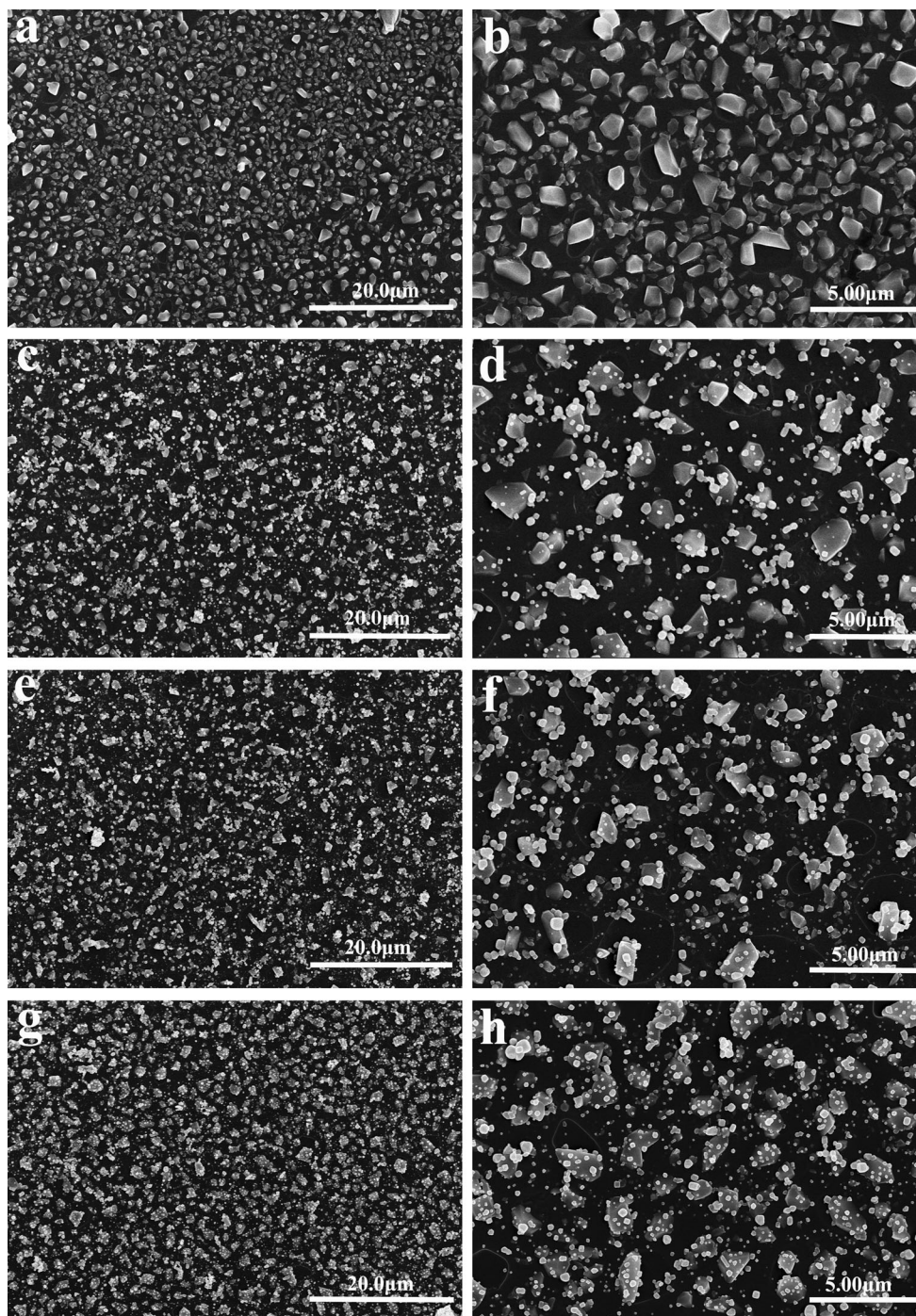
Figure 3 SEM images of pure WO_3 (**a**, **b**), 1-WO_3/Ag/AgCl (**c**, **d**), 2-WO_3/Ag/AgCl (**e**, **f**), 3-WO_3/Ag/AgCl film photocatalysts (**g**, **h**).

band gap energies for pure WO_3 film. The band gap was calculated using Tauc's formula. The band gap for WO_3 film was obtained to be 2.61 eV, which was very close to the previously reported value. [12, 15–17] On account of the enhanced visible light absorption, the photocatalytic activity of the 3-WO_3/ Ag/AgCl film was enhanced with greater utilization of the visible light.

The surface elemental composition and chemical states of the 3-WO_3/Ag/AgCl before and after reuse were investigated by the XPS with the initial pressure of 10^{-8} Pa. The XPS spectra were deconvoluted by using a spectral data processing software, CasaXPS.
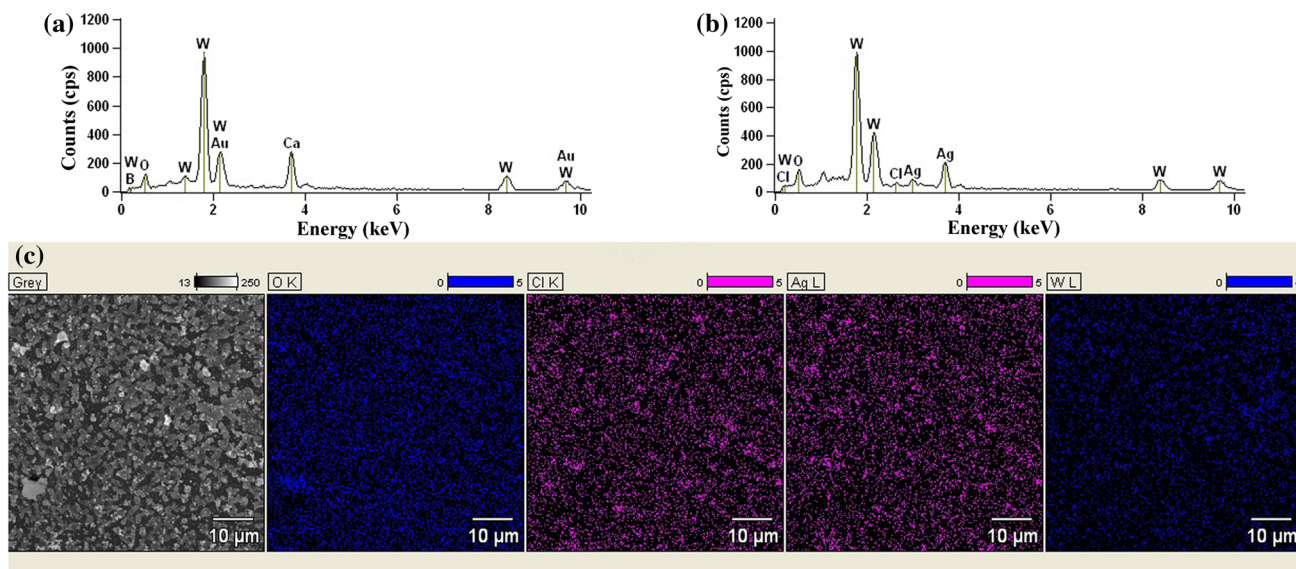
Figure 4 EDS spectrum of pure WO_3 (**a**) and 3-WO_3/Ag/AgCl (**b**) sample, SEM mapping of 3-WO_3/Ag/AgCl (**c**) sample.
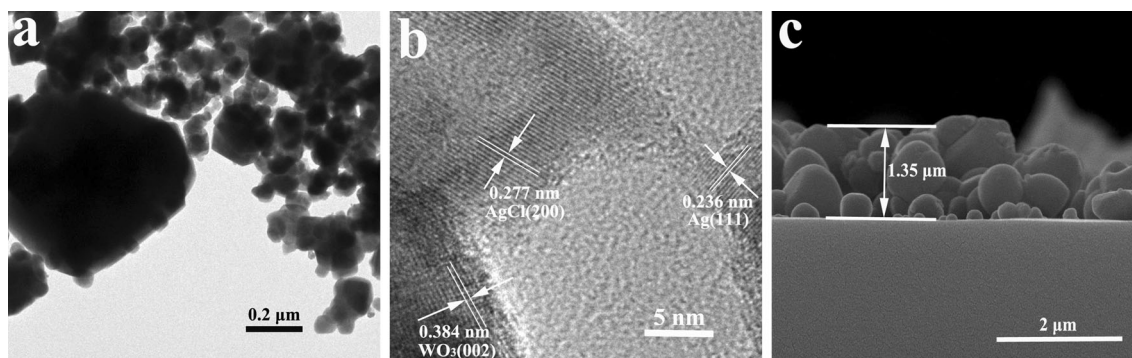
Figure 5 TEM image of 3-WO_3/Ag/AgCl (**a**) HRTEM images of 3-WO_3/Ag/AgCl (**b**) and cross-sectional SEM image of 3-WO_3/Ag/AgCl film (**c**).
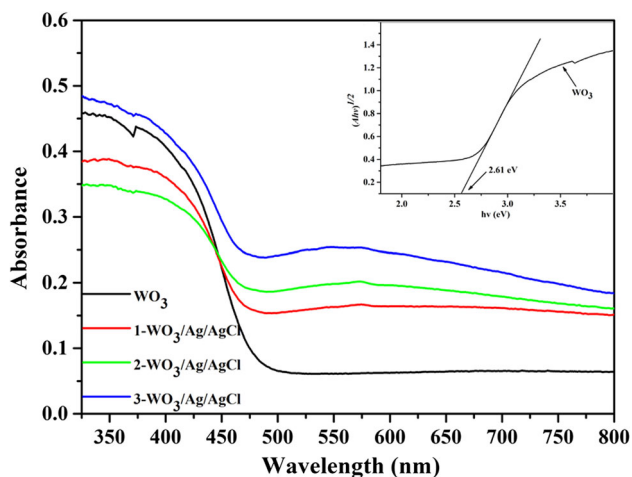
Figure 6 UV–Vis diffuse reflectance spectra of pure WO_3, 1-WO_3/Ag/AgCl, 2-WO_3/Ag/AgCl and 3-WO_3/Ag/AgCl; inset: band gap energies of pure WO_3.

The number and location of the peaks were considered in such a way that the best fit with the original spectrum could be obtained [37, 51–53]. Figure 7a shows the whole XPS spectrum of 3-WO_3/Ag/AgCl before and after reused, and W, O, Ag and Cl are the major elements detected from 3-WO_3/Ag/AgCl. The intensities of the XPS peaks were reduced by around $20\% \pm 10\%$ after five repeated tests. As shown in Fig. 7b, the Ag $3d$ spectrum has two distinct peaks at 367.4 eV and 373.4 eV, and the two peaks can be further deconvoluted into four peaks. These peaks at 367.4 eV and 373.4 eV are ascribed to Ag^+ in AgCl, and the peaks at 368.9 eV and 374.8 eV assigned to Ag^0 [54]. The molar ratio of Ag^+/Ag^0 increased from 0.0469 to 0.0676 after reuse. It was probably due to that Ag^+ was photoreduced into Ag^0 during the repeated photocatalytic process. The peaks of
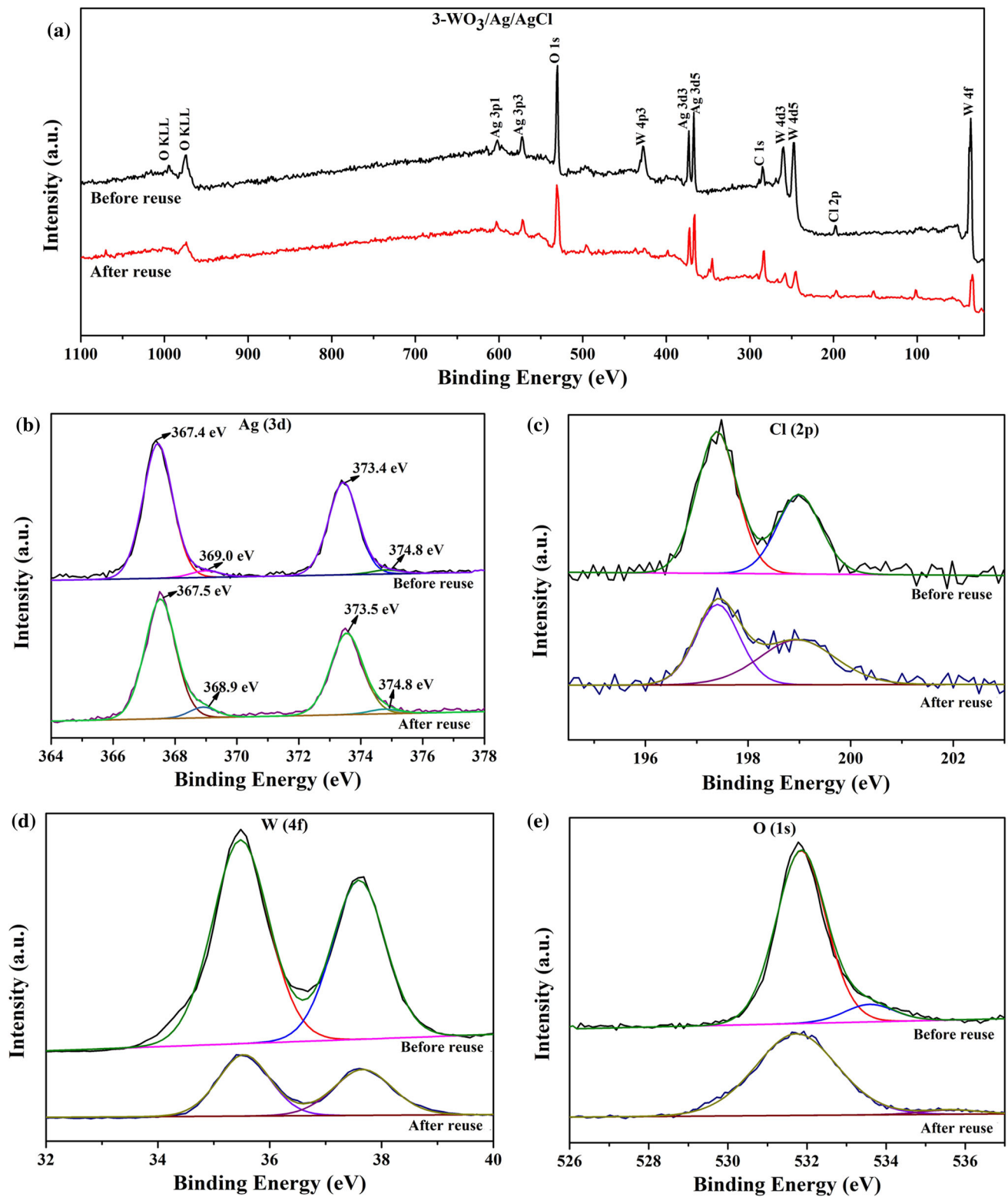
Figure 7 XPS survey spectrum of the 3-WO₃/Ag/AgCl film before reuse and after reuse (**a**), Ag 3d (**b**), Cl 1s (**c**), W 4f (**d**) O 1s and (**e**) high-resolution spectra of 3-WO₃/Ag/AgCl film on glass.

197.4 eV and 198.9 eV belonged to Cl 2p as shown in Fig. 7c, corresponding Cl 2$p_{3/2}$ and Cl 2$p_{1/2}$, respectively. Two main peaks located at 3 5.5 eV and 37.6 eV were ascribed to W 4$f_{7/2}$ and W 4$f_{5/2}$, respectively, of W^{6+} atoms (Fig. 7d). The peak at 531.7 eV belonged to O 1s (Fig. 7e). In addition to the four elements, it can be observed that there were peaks of O KLL and C 1s in the figure. The O KLL is the Auger peak of the O, and the C 1s core level photoemission spectra were deconvoluted to the chemical environments of C atoms from polyvinyl alcohol [37, 51–53].

Photocatalytic activity

MO and RhB have been widely used in various industries such as paper and textiles [55]. MO and RhB were chosen as target pollutants in the evaluation of photocatalytic performances of the as-prepared photocatalysts under visible light ($\lambda > 420$ nm) irradiation. Figure 8a, d shows the degradation rates of MO and RhB in the presence of photocatalyst, where C is the concentration of MO or RhB after a certain irradiation time t and C_0 represents the original concentration of MO or RhB. It is well known that MO and RhB are stable under visible light because the concentration changes of them can be almost neglected after irradiation for a long time in the absence of photocatalysts. From the degradation results, 18.8% of MO was degraded after 180 min and 20.5% of RhB was removed after 150 min by pure WO₃, indicating that the photocatalytic ability of pure WO₃ was very low. However, with the incorporation of Ag and AgCl onto the surface of WO₃, the degradation ability of the WO₃ was greatly improved. As the amount of Ag/AgCl on the WO₃/Ag/AgCl film increased, the degradation ability of photocatalyst also gradually improved. Under visible light irradiation, 3-WO₃/Ag/AgCl film exhibited the best photocatalytic performance for MO and RhB. The degradation percentage of MO after 180 min reached 97.3% and 94.8% for RhB after 150 min. Because AgCl did not absorb visible light, this increase was mainly caused by the SPR effect of the metallic Ag. To get deep insight into the photocatalytic reactions, the relationships between ln(C/C_0) and reaction time t for MO and RhB were investigated. As shown in Fig. 8b, e, the result confirmed that this photocatalytic reaction followed the first-order kinetics as expressed by the equation: ln (C/C_0) = $k_{app}t$, where

t is the reaction time, the C and C_0 are the concentration of MO or RhB at the reaction time t and before the dark absorption, and here k_{app} is the apparent rate constant. From Fig. 8b, e, the 3-WO₃/Ag/AgCl film had the highest photocatalytic performance with $k_{app} = 0.02009$ min^{-1} and $k_{app} = 0.01954$ min^{-1} for MO and RhB, respectively. For WO₃ film, the $k_{app} = 0.00111$ min^{-1} and $k_{app} = 0.00152$ min^{-1} for MO and RhB, respectively. The results were consistent with the previous photocatalytic degradation experiments. As shown in Fig. 8c, f, the absorption spectral intensity of MO and RhB under visible light reduced gradually with the irradiation time over 3-WO₃/Ag/AgCl,consistent with the results of degradation tests.

The stability of photocatalyst is an important factor for the performance evaluation for the catalyst, and this is also an important criterion whether the photocatalyst has practical applications. The reusability of 3-WO₃/Ag/AgCl film was evaluated by repeating degradation experiments of MO and RhB for five times under visible light. After each cycle, the photocatalyst was washed with deionized for several times and dried at 80 °C for 1 h. Figure 9a, b shows that after five cyclic degradation experiments, the photocatalytic activity of 3-WO₃/Ag/AgCl exhibited virtually no deteriorated evidence. In particular, as shown in Fig. 9b, c, the SEM of 3-WO₃/Ag/AgCl film that after five cyclic degradation experiments was almost unchanged compared with the prepared sample. These results indicated a good stability and reusability for degrading MO and RhB by the films.

Photocatalytic mechanism

The photochemical tests are effective means for studying the electrochemical interfacial performances of the samples [35]. The interface charge separation and transport of the photo-generated electrons and holes is an important factor for the photocatalytic properties. In this study, EIS was used to investigate the charge separation efficiency. As shown in Fig. 10a, the arc radius of the WO₃/Ag/AgCl photocatalysts was observed to be smaller than the pure WO₃ photocatalyst. It is generally accepted that a smaller the arc radius corresponds a higher the charge separation efficiency and lower charge transfer resistance of the heterojunction [56]. This result shows that Ag and AgCl greatly promoted the separation of photo-generated electron–hole pairs and improved the charge transfer efficiency of WO₃.
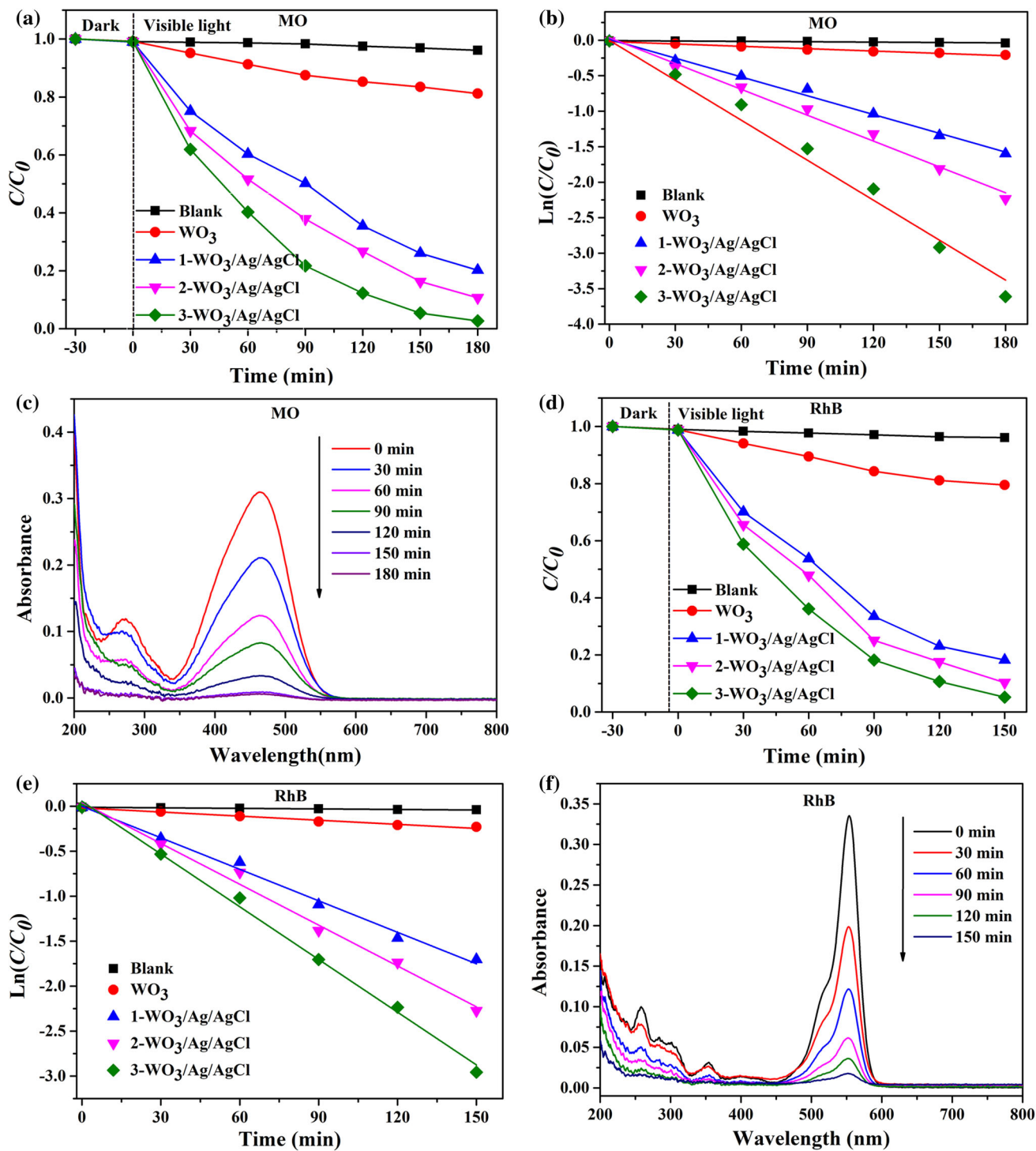
Figure 8 Photocatalytic degradation rates of different catalysts on the degradation of MO (**a**) and RhB (**d**) under visible light; plots of $\ln(C/C_0)$ against reaction time of different photocatalysts for the degradation of MO (**b**) and (**e**); time-dependent UV–Vis absorption spectra for the degradations of MO (**c**) and RhB (**f**) over 3-WO$_3$/Ag/AgCl catalyst.

To further explore the photoelectric property of photocatalysts under visible light, the transient photocurrent responses were performed with typical six light on–off cycles of 30-s interval under visible light. In general, the higher the photoelectric current intensity, the higher the efficiency of photo-generated
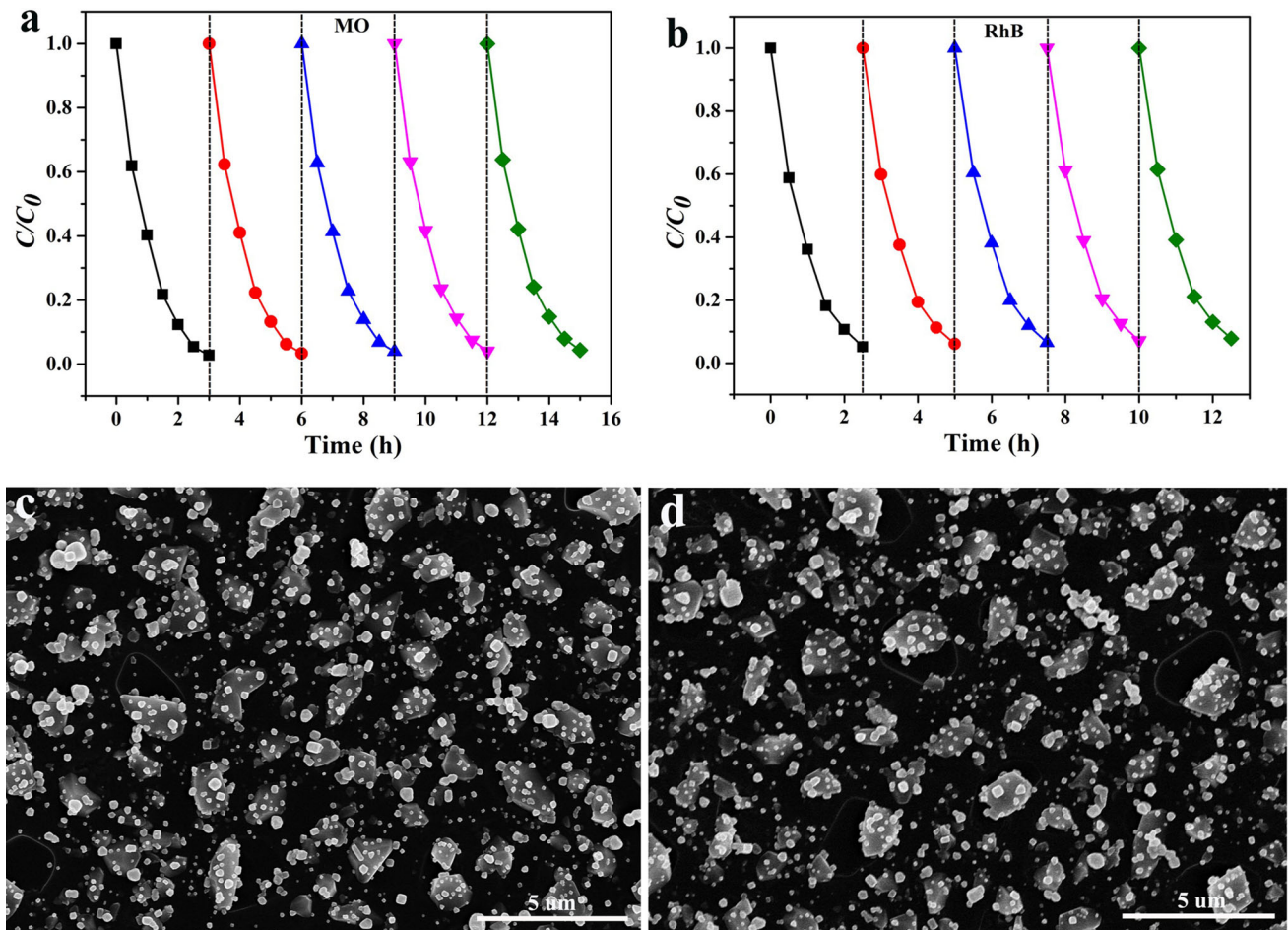
Figure 9 Five photodegradation cycles of MO (**a**) and RhB (**b**) over the 3-WO$_3$/Ag/AgCl film catalyst and the SEM images of 3-WO$_3$/Ag/AgCl film before (**c**) and after (**d**) being reused under visible light irradiation.
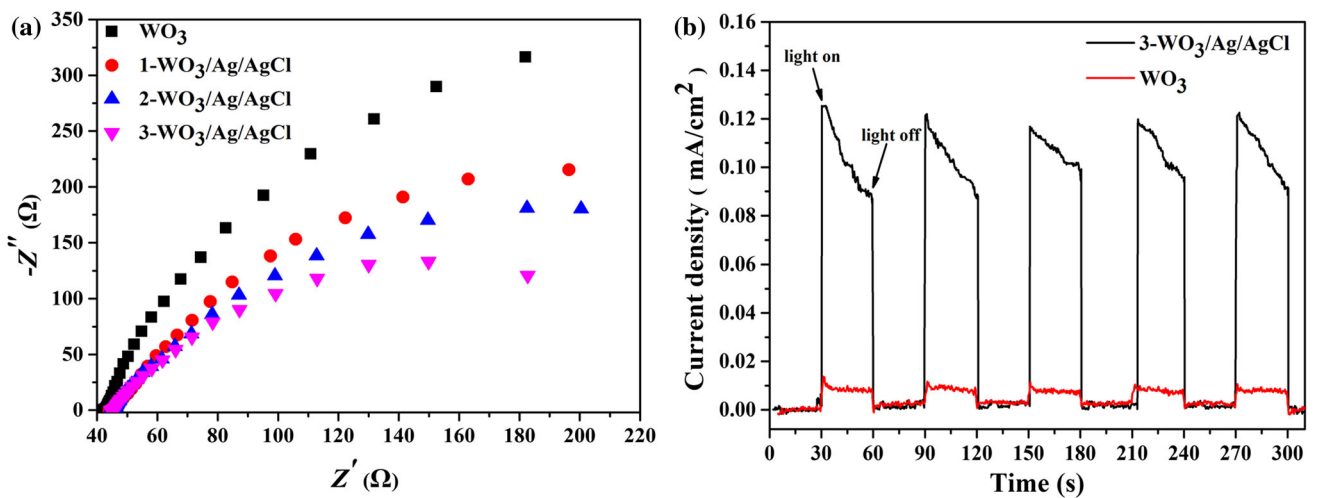

Figure 10 EIS Nyquist plots of WO$_3$ and three WO$_3$/Ag/AgCl samples (**a**) transient photocurrent responses of WO$_3$ and 3-WO$_3$/Ag/AgCl under visible light illumination (**b**).

electron and hole separation of photocatalysts, and the better photocatalytic performance [57]. As shown in Fig. 10b, when the visible light is applied, the photocurrent increased instantly and decreased slightly with the irradiation time. The photocurrent quickly dropped to zero once the light was cut off. The photocurrent of 3-WO$_3$/Ag/AgCl film sample is about 13 times larger than that of WO$_3$ under visible light. It is generally accepted that a larger photocurrent density signifies a more efficient electron transfer and a slower recombination of photo-generated electron and hole [58]. The result is regarded as a further evidence that Ag/AgCl could promote the electron transfer and separation of photo-generated electron and hole. This result is consistent with the previous EIS result.

It is well known that the reactive oxygen species (ROSs) in photocatalyst such as ·OH, h$^+$ and ·O$_2^-$ play a critical role in the photodegradation of dye pollutants [59]. To determine the ROSs in the photocatalytic process, several scavengers were employed in the degradation experiments with 3-WO$_3$/Ag/AgCl film of MO and RhB under visible light. 2 mM isopropyl alcohol (IPA), 1,4-benzoquinone (BQ) and ethylenediaminetetraacetic acid disodium salt (EDTA-2Na) were used as scavengers of ·OH, h$^+$ and ·O$_2^-$, respectively [42–45]. As shown in Fig. 11a, b, after the addition of IPA, the degradation efficiency difference of MO and RhB was almost not noticeable, indicating that ·OH had no influence in the process of catalytic degradation. However, the photodegradation of MO and RhB were inhibited to varied degrees compared with no

scavengers when in the presence of BQ and EDTA-2Na. EDTA-2Na had the best inhibition effect on photodegradation of MO and RhB. This result shows that ·O$_2^-$ and h$^+$ play the major roles in photodegradation, while the effect of ·OH could be neglected.

To further analyze the photocatalytic mechanism, the conductor band (CB) and valence (VB) potentials of WO$_3$ can be calculated by following empirical equations [60]:

$$E_{VB} = X - E_e + 0.5E_g$$

$$E_{CB} = E_{VB} - E_g$$

Here, E_e and E_g are the energy of free electrons (4.50 eV vs SHE) on the hydrogen scale and E_{VB} is the valence band energy level [44]. X is the absolute electronegativity. In this work, the X value is 6.49 eV for pure WO$_3$ [61]. From Fig. 6, E_g value is 2.61 eV from the DRS results. According to the above results, the VB and CB energies of WO$_3$ are calculated to be 3.3 eV and 0.69 eV versus SHE.

Accordingly, a Z-scheme photocatalytic mechanism is proposed for WO$_3$/Ag/AgCl, as shown in Fig. 12. WO$_3$ with a band gap of 2.61 eV can generate the electron pairs and hole under the visible light illumination, while AgCl with a band gap of 3.25 eV cannot be excited. In the Z-scheme WO$_3$–Ag–AgCl system, Ag NPs serve as the electron mediator. The photo-generated electrons in the CB of WO$_3$ combine with the plasmon-generated holes of Ag NPs. Meanwhile, the plasmon-induced electrons will be injected into the CB of AgCl. This is consistent with
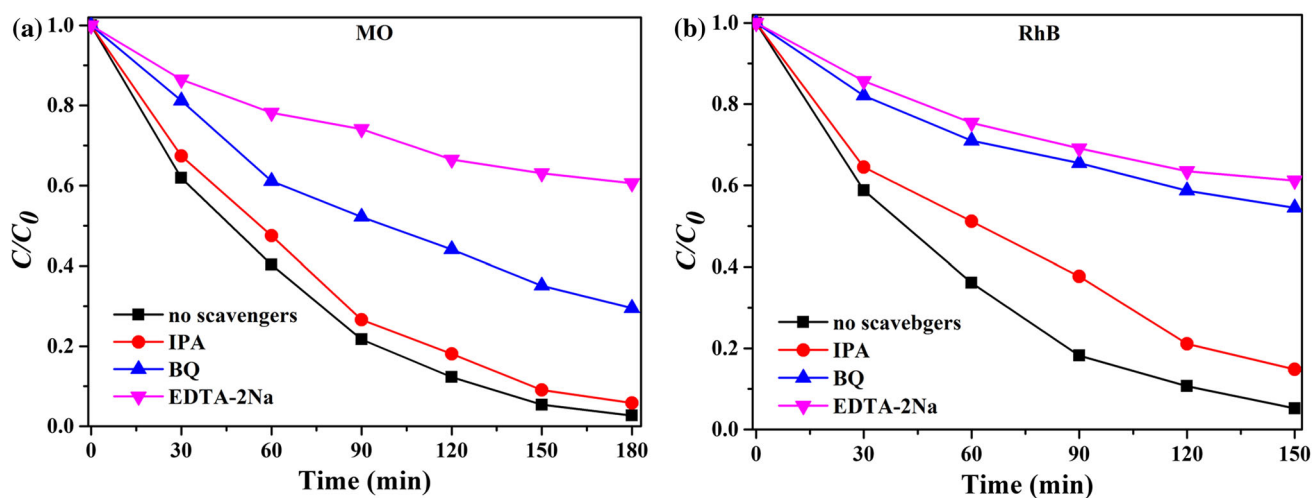

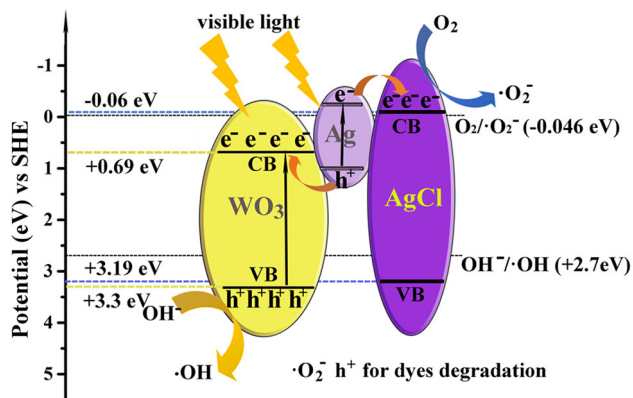**Figure 11** Photocatalytic degradation plots of MO (**a**) and MO (**b**) on 3-WO$_3$/Ag/AgCl under different conditions.

Figure 12 The possible photocatalytic mechanism of organic pollutants degradation on WO$_3$/Ag/AgCl film under visible light illumination.

the previously reported AgCl–Ag–H$_2$WO$_4$·H$_2$O and AgCl–Ag–Bi$_{20}$TiO$_{32}$ systems [61, 62]. The conduction edge potential of AgCl ($-$ 0.06 eV vs SHE) is more negative than the reduction potential of O$_2$/·O$_2^-$ ($-$ 0.046 eV vs SHE) allowing O$_2$ reduction. The valence band of WO$_3$ (3.3 eV) is positioned at a more positive potential with respect to the couple OH$^-$/ ·OH ($+$ 2.70 eV vs SHE). The holes in the VB of WO$_3$ can directly oxidize the dye molecule and oxidize H$_2$O to ·OH. Accordingly, the oxidation active sites are on the VB of WO$_3$, and the reduction active sites are on the CB of AgCl [63]. The Z-scheme WO$_3$–Ag– AgCl system enables the spatial isolation of photo-generated electrons and holes, thus reducing the bulk electron–hole recombination. In this way, the photo-catalytic performance of the WO$_3$/Ag/AgCl photo-catalyst has been significantly improved.

Conclusions

In summary, we successfully prepared WO$_3$ film photocatalyst on glass by a spin coating method. Various WO$_3$/Ag/AgCl film photocatalysts were prepared by an impregnating–precipitation–pho-toreduction method with different concentrations of AgNO$_3$ and NaCl solutions. The as-prepared photo-catalyst displayed the excellent photocatalytic per-formance under visible light illumination. Meanwhile, the photocatalyst had excellent stability and reusability. The Z-scheme mechanism for WO$_3$/ Ag/AgCl was proposed based on the photoelectro-chemical test and radical trapping measurement. The study offers a practical photocatalyst and may also

provide a methodology for preparing various pho-tocatalysts, on other substrates, e.g., on ceramics or metals.

References

[1] Jones VJ, Rose NL, Self AE, Solovieva N, Yang H (2015) Evidence of global pollution and recent environmental change in Kamchatka, Russia. Glob Planet 134:82–90

[2] Zhu Z, Yan Y, Li J (2016) One-step synthesis of flower-like WO$_3$/Bi$_2$WO$_6$, heterojunction with enhanced visible light photocatalytic activity. J Mater Sci 51:2112–2120. https://d oi.org/10.1007/s10853-015-9521-z

[3] Low J, Cheng B, Yu J (2017) Surface modification and enhanced photocatalytic CO$_2$ reduction performance of TiO$_2$: a review. Appl Surf Sci 392:658–686

[4] Chatterjee D, Dasgupta S (2005) Visible light induced pho-tocatalytic degradation of organic pollutants. J Photochem Photobiol C 6:186–205

[5] Yu CJ, Zhang L, Yu J (2002) Rapid synthesis of mesoporous TiO$_2$ with high photocatalytic activity by ultrasound-induced agglomeration. New J Chem 26:416–420

[6] Chai SY, Kim YJ, Jung MH, Chakraborty AK, Jung D, Lee WI (2009) Heterojunctioned BiOCl/Bi$_2$O$_3$, a new visible light photocatalyst. J Catal 262:144–149

[7] Carvalho HWP, Batista APL, Bertholdo R, Santilli CV, Pulcinelli SH, Ramalho TC (2010) Photocatalyst TiO$_2$–Co: the effect of doping depth profile on methylene blue degra-dation. J Mater Sci 45:5698–5703. https://doi.org/10.1007/ s10853-010-4639-5

[8] Wang Y, Shi R, Lin J, Zhu Y (2011) Enhancement of pho-tocurrent and photocatalytic activity of ZnO hybridized with graphite-like C$_3$N$_4$. Energy Environ Sci 4:2922–2929

[9] Iskandar F, Nandiyanto ABD, Yun KM, Hogan CJ, Okuyama K, Biswas P (2007) Enhanced photocatalytic

performance of brookite TiO_2 macroporous particles prepared by spray drying with colloidal templating. Adv Mater 19:1408–1412

[10] Ohno Teruhisa, Mitsui Takahiro, Matsumura Michio (2003) Photocatalytic activity of S-doped TiO_2 photocatalyst under visible light. Chem Lett 32:364–365

[11] O'regan B, Grätzel M (1991) A low-cost, high-efficiency solar cell based on dye-sensitized colloidal TiO_2 films. Nature 353:737–740

[12] Zhu W, Liu J, Yu S, Zhou Y, Yan X (2016) Ag loaded WO_3 nanoplates for efficient photocatalytic degradation of sulfanilamide and their bactericidal effect under visible light irradiation. J Hazard Mater 318:407–416

[13] Ma B, Guo J, Dai WL, Fan K (2012) Ag–AgCl/WO_3 hollow sphere with flower-like structure and superior visible photocatalytic activity. Appl Catal B 123:193–199

[14] Zhou J, Cheng Y, Yu J (2011) Preparation and characterization of visible-light-driven plasmonic photocatalyst Ag/AgCl/TiO_2 nanocomposite thin films. J Photochem Photobiol A 223:82–87

[15] Abe R, Takami H, Murakami N, Ohtani B (2008) Pristine simple oxides as visible light driven photocatalysts: highly efficient decomposition of organic compounds over platinum-loaded tungsten oxide. J Am Chem Soc 130:7780–7781

[16] Chen D, Gao L, Yasumori A, Kuroda K, Sugahara Y (2008) Size-and shape-controlled conversion of tungstate-based inorganic–organic hybrid belts to WO_3 nanoplates with high specific surface areas. Small 4:1813–1822

[17] Ham DJ, Phuruangrat A, Thongtem S, Lee JS (2010) Hydrothermal synthesis of monoclinic WO_3 nanoplates and nanorods used as an electrocatalyst for hydrogen evolution reactions from water. Chem Eng J 165:365–369

[18] Tong M, Dai G, Wu Y, He X, Gao D (2001) WO_3 thin film prepared by PECVD technique and its gas sensing properties to NO_2. J Mater Sci 36:2535–2538. https://doi.org/10.1023/A:1017950619864

[19] Deepa M, Sharma N, Varshney P, Varma SP, Agnihotry SA (2000) FTIR investigations of solid precursor materials for sol-gel deposition of WO_3 based electrochromic films. J Mater Sci 35:5313–5318. https://doi.org/10.1023/A:1004838627252

[20] Bose RJ, Illyasukutty N, Tan KS, Rawat RS, Matham MV, Kohler H, Pillai VPM (2018) Preparation and characterization of Pt loaded WO_3 films suitable for gas sensing applications. Appl Surf Sci 440:320–330

[21] Yan Z, Wei W, Xie J, Meng S, Lü X, Zhu J (2013) An ion exchange route to produce WO_3 nanobars as Pt electrocatalyst promoter for oxygen reduction reaction. J Power Sources 222:218–224

[22] Zhu W, Liu J, Yu S, Zhou Y, Yan X (2016) Ag loaded WO_3 nanoplates for efficient photocatalytic degradation of sulfanilamide and their bactericidal effect under visible light irradiation. J Hazard Mater 318:407–416

[23] Katsumata H, Oda Y, Kaneco S, Suzuki T (2013) Photocatalytic activity of Ag/CuO/WO_3 under visible-light irradiation. RSC Adv 3:5028–5035

[24] Zhang T, Zhu Z, Chen H, Bai Y, Xiao S, Zheng X, Yang S (2015) Iron-doping-enhanced photoelectrochemical water splitting performance of nanostructured WO_3: a combined experimental and theoretical study. Nanoscale 7:2933–2940

[25] Sun Y, Murphy CJ, Reyes-Gil KR, Reyes-Garcia EA, Thornton JM, Morris NA, Raftery D (2009) Photoelectrochemical and structural characterization of carbon-doped WO_3 films prepared via spray pyrolysis. Int J Hydrog Energy 34:8476–8484

[26] Iskandar F, Nandiyanto ABD, Yun KM, Hogan CJ, Okuyama K, Biswas P (2007) Enhanced photocatalytic performance of brookite TiO_2 macroporous particles prepared by spray drying with colloidal templating. Adv Mater 19:1408–1412

[27] Khan SU, Al-Shahry M, Ingler WB (2002) Efficient photochemical water splitting by a chemically modified n-TiO_2. Science 297:2243–2245

[28] Yu JC, Yu J, Ho W, Jiang Z, Zhang L (2002) Effects of F-doping on the photocatalytic activity and microstructures of nanocrystalline TiO_2 powders. Chem Mater 14:3808–3816

[29] Ye L, Liu J, Gong C, Tian L, Peng T, Zan L (2012) Two different roles of metallic Ag on Ag/AgX/BiOX (X = Cl, Br) visible light photocatalysts: surface plasmon resonance and Z-scheme bridge. ACS Catal 2:1677–1683

[30] Yu J, Sun D, Wang T, Li F (2018) Fabrication of Ag@AgCl/ZnO submicron wire film catalyst on glass substrate with excellent visible light photocatalytic activity and reusability. Chem Eng J 334:225–236

[31] Liu S, Yu J, Wang T, Li F (2017) A multifunctional Ag/PAOCG reusable substrate for p-nitrophenol reduction and SERS applications. J Mater Sci 52:13736–13748. https://doi.org/10.1007/s10853-017-1461-3

[32] Yu J, Yang J, Sun D, Wang T (2016) A novel nanoporous surface for immobilization and expression of functional chemicals. Mater Lett 180:148–152

[33] Zhang S, Li J, Wang X, Huang Y, Zeng M, Xu J (2014) In situ ion exchange synthesis of strongly coupled Ag@AgCl/g-C_3N_4 porous nanosheets as plasmonic photocatalyst for highly efficient visible-light photocatalysis. ACS Appl Mater Interfaces 6:22116–22125

[34] Ye L, Liu J, Gong C, Tian L, Peng T, Zan L (2012) Two different roles of metallic Ag on Ag/AgX/BiOX (X = Cl,

Br) visible light photocatalysts: surface plasmon resonance and Z-scheme bridge. ACS Catal 2:1677–1683

[35] Li H, Sun Y, Cai B, Gan S, Han D, Niu L, Wu T (2015) Hierarchically Z-scheme photocatalyst of Ag@AgCl decorated on BiVO₄ (0 4 0) with enhancing photoelectrochemical and photocatalytic performance. Appl Catal B 170:206–214

[36] Gao L, Gan W, Cao G, Zhan X, Qiang T, Li J (2017) Visible-light activate Ag/WO₃ films based on wood with enhanced negative oxygen ions production properties. Appl Surf Sci 425:889–895

[37] Hashemi A, Bahari A, Ghasemi S (2018) Effect of annealing treatment on optical properties and microstructural variation of WO₃/Ag/WO₃ multilayer nano-films. Bull Mater Sci 41:45

[38] Ma B, Guo J, Dai WL, Fan K (2012) Ag–AgCl/WO₃ hollow sphere with flower-like structure and superior visible photocatalytic activity. Appl Catal B 123:193–199

[39] Adhikari R, Gyawali G, Sekino T, Lee SW (2013) Microwave assisted hydrothermal synthesis of Ag/AgCl/WO₃ photocatalyst and its photocatalytic activity under simulated solar light. J Solid State Chem 197:560–565

[40] Feng Z, Yu J, Sun D, Wang T (2016) Visible-light-driven photocatalysts Ag/AgCl dispersed on mesoporous Al₂O₃ with enhanced photocatalytic performance. J Colloid Interface Sci 480:184–190

[41] Tang Y, Jiang Z, Deng J, Gong D, Lai Y, Tay HT, Chen Z (2012) Synthesis of nanostructured silver/silver halides on titanate surfaces and their visible-light photocatalytic performance. ACS Appl Mater Interfaces 4:438–446

[42] Yang X, Tang H, Xu J, Antonietti M, Shalom M (2015) Silver phosphate/graphitic carbon nitride as an efficient photocatalytic tandem system for oxygen evolution. Chemsuschem 8:1350–1358

[43] Ma BC, Ghasimi S, Landfester K, Vilela F, Zhang KA (2015) Conjugated microporous polymer nanoparticles with enhanced dispersibility and water compatibility for photocatalytic applications. J Mater Chem A 3:16064–16071

[44] Lv X, Wang T, Jiang W (2018) Preparation of Ag@AgCl/g-C₃N₄/TiO₂ porous ceramic films with enhanced photocatalysis performance and self-cleaning effect. Ceram Int 44:9326–9337

[45] Liao W, Zhang Y, Zhang M, Murugananthan M, Yoshihara S (2013) Photoelectrocatalytic degradation of microcystin-LR using Ag/AgCl/TiO₂ nanotube arrays electrode under visible light irradiation. Chem Eng J 231:455–463

[46] Yang Y, Zhang Y, Dong M, Yan T, Zhang M, Zeng Q (2017) Highly efficient degradation of thidiazuron with Ag/AgCl-activated carbon composites under LED light irradiation. J Hazard Mater 335:92–99

[47] Huang W, Jing C, Zhang X, Tang M, Tang L, Wu M, Liu N (2018) Integration of plasmonic effect into spindle-shaped MIL-88A (Fe): steering charge flow for enhanced visible-light photocatalytic degradation of ibuprofen. Chem Eng J 349:603–612

[48] Yao X, Liu X (2014) One-pot synthesis of ternary Ag₂CO₃/Ag/AgCl photocatalyst in natural geothermal water with enhanced photocatalytic activity under visible light irradiation. J Hazard Mater 280:260–268

[49] Zhan F, Yang Y, Li W, Li J, Liu W, Li Y, Chen Q (2016) Preparation of DyVO₄/WO₃ heterojunction plate array films with enhanced photoelectrochemical activity. RSC Adv 6:10393–10400

[50] Tanaka A, Hashimoto K, Kominami H (2014) Visible-light-induced hydrogen and oxygen formation over Pt/Au/WO₃ photocatalyst utilizing two types of photoabsorption due to surface plasmon resonance and band-gap excitation. J Am Chem Soc 136:586–589

[51] Hashemi A, Bahari A, Ghasemi S (2018) Synthesis and characterization of cross-linked nanocomposite as a gate dielectric for p-type silicon field-effect transistor. J Electron Mater 47:3717–3726

[52] Hashemi A, Bahari A, Ghasemi S (2017) The low threshold voltage n-type silicon transistors based on a polymer/silica nanocomposite gate dielectric: the effect of annealing temperatures on their operation. Appl Surf Sci 416:234–240

[53] Hashemi A, Bahari A, Ghasemi S (2017) Reduction the leakage current through povidone-SiO₂ nano-composite as a promising gate dielectric of FETs. J Mater Sci Mater Electron 28:13313–13319

[54] Zhu M, Chen P, Liu M (2011) Graphene oxide enwrapped Ag/AgX (X = Br, Cl) nanocomposite as a highly efficient visible-light plasmonic photocatalyst. ACS Nano 5:4529–4536

[55] Chen T, Zheng Y, Lin JM, Chen G (2008) Study on the photocatalytic degradation of methyl orange in water using Ag/ZnO as catalyst by liquid chromatography electrospray ionization ion-trap mass spectrometry. J Am Soc Mass Spectrom 19:997–1003

[56] Shi W, Zhang X, Brillet J, Huang D, Li M, Wang M, Shen Y (2016) Significant enhancement of the photoelectrochemical activity of WO₃ nanoflakes by carbon quantum dots decoration. Carbon 105:387–393

[57] Cui L, Ding X, Wang Y, Shi H, Huang L, Zuo Y, Kang S (2017) Facile preparation of Z-scheme WO₃/g-C₃N₄ composite photocatalyst with enhanced photocatalytic performance under visible light. Appl Surf Sci 391:202–210

[58] Shi L, Liang L, Ma J, Meng Y, Zhong S, Wang F, Sun J (2014) Highly efficient visible light-driven Ag/AgBr/ZnO

composite photocatalyst for degrading Rhodamine B. Ceram Int 40:3495–3502

[59] Liang Y, Lin S, Liu L, Hu J, Cui W (2015) Oil-in-water self-assembled Ag@AgCl QDs sensitized Bi_2WO_6: enhanced photocatalytic degradation under visible light irradiation. Appl Catal B 164:192–203

[60] Chen S, Hu Y, Meng S, Fu X (2014) Study on the separation mechanisms of photogenerated electrons and holes for composite photocatalysts $g-C_3N_4–WO_3$. Appl Catal B 150:564–573

[61] Wang X, Li S, Ma Y, Yu H, Yu J (2011) $H_2WO_4 \cdot H_2O/Ag/AgCl$ composite nanoplates: a plasmonic Z-scheme visible-light photocatalyst. J Phys Chem C 115:14648–14655

[62] Hou J, Wang Z, Yang C, Zhou W, Jiao S, Zhu H (2013) Hierarchically plasmonic Z-scheme photocatalyst of Ag/AgCl nanocrystals decorated mesoporous single-crystalline metastable $Bi_{20}TiO_{32}$ nanosheets. J Phys Chem C 117:5132–5141

[63] Kumar SG, Rao KK (2015) Tungsten-based nanomaterials (WO_3 & Bi_2WO_6): modifications related to charge carrier transfer mechanisms and photocatalytic applications. Appl Surf Sci 355:939–958